Journal of Materials Science: Materials in Electronics (2018) 29:5253–5263
https://doi.org/10.1007/s10854-017-8489-7

Microstructural evolution of 96.5Sn–3Ag–0.5Cu lead free solder reinforced with nickel-coated graphene reinforcements under large temperature gradient

Guang Chen[1,2] · Li Liu[2] · Vadim V. Silberschmidt[2] · Changqing Liu[2] · Fengshun Wu[1] · Y. C. Chan[3]

Received: 6 August 2017 / Accepted: 27 December 2017 / Published online: 6 January 2018
© The Author(s) 2018. This article is an open access publication

Abstract

In this study, 96.5Sn–3Ag–0.5Cu (SAC305) lead-free composite solder containing graphene nanosheets (GNS) decorated with Ni nanoparticles (Ni-GNS) was prepared using a powder metallurgy method. A lab-made set-up and a corresponding Cu/solder/Cu sample design for assessing thermo-migration (TM) was established. The feasibility of this setup for TM stressing using an infrared thermal imaging method was verified; a temperature gradient in a solder joint was observed at 1240 K/cm. Microstructural evolution and diffusion of Cu in both plain and composite solder joints were then studied under TM stressing conditions. Compared to unreinforced SAC305 solder, the process of diffusion of Cu atoms in the composite solder joint was significantly reduced. The interfacial intermetallic compounds (IMCs) present in the composite solder joint also provide a more stable morphology after the TM test for 600 h. Furthermore, during the TM test, the Ni-GNS reinforcement affects the formation, migration and distribution of Ni–Cu–Sn and Cu–Sn IMCs by influencing the dissolution rate of Cu atoms.

1 Introduction

The 96.5Sn–3Ag–0.5Cu ternary alloy is currently regarded as a promising substitution for traditional Sn–Pb solder within the electronic packaging industry owing to its environmentally-friendly and outstanding mechanical properties and good solderability [1–3]. However, with constant developments in miniaturization and integration density in high-density electronic packages, electro- and thermo-migration (TM) failures induced by high current density and large thermal gradients are becoming a prominent issue and reliability concern in solder interconnections [4–6]. Research shows that an instance of high joule heat and large temperature gradient are more likely to cause failure in solder joints [4]. Thus, with the trend towards decreasing interconnection size, the service reliability of lead-free solder interconnections will be increasingly threatened by electro-migration (EM) and in particular, TM.

Previous studies indicate that solderability and mechanical properties of existing lead-free solders could be improved by the inclusion of suitable foreign reinforcement into the solder matrix to prepare a composite solder; the materials added could be metallic, ceramic, rare earth elements and carbon-based nanomaterials [7–11]. Gao et al. [7] studied the effect of foreign metal particles and rare earth elements added to microstructures and properties of Sn–Ag–Cu solders, and proposed that a small amount of Zn addition shows a desired tendency to reduce undercooling, while an appropriate amount of Bi, Ni or Ga enhances the wettability of Sn–Ag–Cu solders. Moreover, doping of Co, Fe or Ge has the positive effect of microstructural refinement. Tsao et al. [8] reported that ultimate tensile strength (UTS), Young's modulus (YS), and microhardness of the Sn1.5Sb1Ag composite solder were effectively improved by adding 0.75 wt% TiO_2 nano-particles. Using the powder metallurgical method, Sn58Bi0.7Zn composite solders containing graphene nanosheets were prepared by Ma et al. [9], who found that the composite

✉ Changqing Liu
C.Liu@lboro.ac.uk

✉ Fengshun Wu
fengshunwu@hust.edu.cn

[1] State Key Laboratory of Materials Processing and Die & Mould Technology, Huazhong University of Science and Technology, Wuhan 430074, China

[2] Wolfson School of Mechanical, Electrical and Manufacturing Engineering, Loughborough University, Loughborough, UK

[3] Department of Electronic Engineering, City University of Hong Kong, Tat Chee Avenue, KowLoon Tong, Hong Kong

solder joints exhibited a better creep resistancy and UTS with suppressed interfacial IMC layers.

In addition to investigations on the physical and mechanical properties of composite solders, other researchers have studied the effect of added reinforcement to provide service reliability of solder joints under high current stressing; findings suggest that a suitable type of doped reinforcement, used in an appropriate amount, could help to mitigate the failure of solder joints induced by EM behaviour [12, 13]. Despite TM behavior in a plain solder joint being reported previously [14, 15], up until the current time a systematic study of microstructural evolution and elemental redistribution in a composite solder interconnection containing enhancing particles involving a large temperature gradient is still absent.

In contrast to commonly mentioned foreign reinforcement materials (e.g. Ni, Cu, Ag, Al_2O_3, ZrO_2, Carbon nanotubes and graphene), our research group prepared a novel reinforcement material—Ni-coated graphene, by means of an electroless plating method [16]. This composite reinforcement is expected to provide a solution to certain disadvantages of using metal (for example coarsening during thermal ageing) and nonmetal reinforcement (hardly to be reactively wetted by molten solder) [17–19]. The Ni nanoparticles deposited upon the surface of GNS could serve as a 'bridge', which could link the GNS sheets and solder matrix by forming a Ni-containing IMC around the GNS. This experiment showed that the thickness and morphology of interfacial IMC between the solder and Cu substrate were changed, while the mechanical properties of the composite solder joints (including their microhardness and shear strength) were considerably improved following the addition of Ni-GNS reinforcement [16].

To further investigate the influence of Ni-GNS on TM behavior of solder joints, in this paper, a SAC/0.1Ni-GNS composite solder was similarly manufactured using the powder metallurgy process. A sandwich-like Cu/Solder/Cu sample was then prepared for subsequent TM stressing. It is widely reported that TM in Sn-based solder alloys can be triggered when an environmental temperature and a temperature gradient reach at least 100 °C and 1000 K/cm, respectively [14]. Therefore in this study, in order to achieve a sufficiently high environmental temperature and thermal gradient without involving the influence of EM, a set-up for TM stressing based on a Peltier thermoelectric cooler and a heating plate with a constant temperature was designed and prepared. Feasibility of this particular set-up and corresponding samples was also experimentally verified. After different TM stressing times, microstructural evolution of both plain and composite solder joints (including center and interfacial areas) were comparatively studied and discussed. Moreover, the dissolution rate of Cu atoms (from Cu substrate to solder) under current experimental conditions was also quantitatively evaluated.

2 Experimental

2.1 Materials

SAC305 (wt%) lead-free solder powder with diameter of 25–45 µm was provided by Beijing Compo, China; multilayer GNS nanosheets were purchased from JCNANO Materials Tech (China) at a size of 3–10 µm and thickness of 5–10 nm. GNS nanosheets coated with Ni nanoparticles were then prepared using the chemical reduction method [16]. The SEM image of as-purchased GNS nano-sheets is shown in Fig. 1a; from the corresponding Raman spectrum shown in Fig. 1b, three peaks are notable: 1363, 1586 and 2720 cm^{-1}, which are characteristics of GNS [20]. The SEM image and corresponding EDX result of as-prepared Ni-GNS shown in Fig. 1c, d indicate that Ni nanoparticles with an average diameter of 100 nm were successfully deposited on the surface of GNSs. In addition, the Ni-GNS reinforcements prepared tend to absorb organic functional groups or small molecules (such as oxygen) from air environment because of theirs large specific surface area, leading to N and O were detected from EDX test. The purchased SAC305 solder powder and the as-prepared Ni-GNS were used as materials in their original form.

2.2 Preparation of composite solder

To synthesize the composite solder, the pre-weighted Ni-GNS reinforcement (0.1 wt%) and SAC305 solder powder (99.9 wt%) were first homogenously blended in a planetary ball mill at the speed of 150 rpm for 20 h. This mixture was then compacted into solder billets before being sintered at 180 °C for 3 h in a vacuum atmosphere. Finally the sintered solder billets were rolled into solder foils, each with a thickness of 100 µm.

2.3 Preparation of TM setup and sample

A lab-designed set-up for TM stressing was developed, which can be seen in Fig. 2. The TM stressing system consisted of a Peltier thermoelectric device for cooling and a constant-temperature heating plate set to a temperature of 250 ± 5 °C. The temperature controller was placed in series with the thermoelectric cooler to guarantee a relatively stable initial temperature (0 ± 2 °C), while a heat sink and cooling fan were employed to ensure the thermoelectric cooler works effectively during the stressing process. The heating and cooling components were then fixed on corresponding Cu bases; the thickness of Cu base is 8 mm and it is used

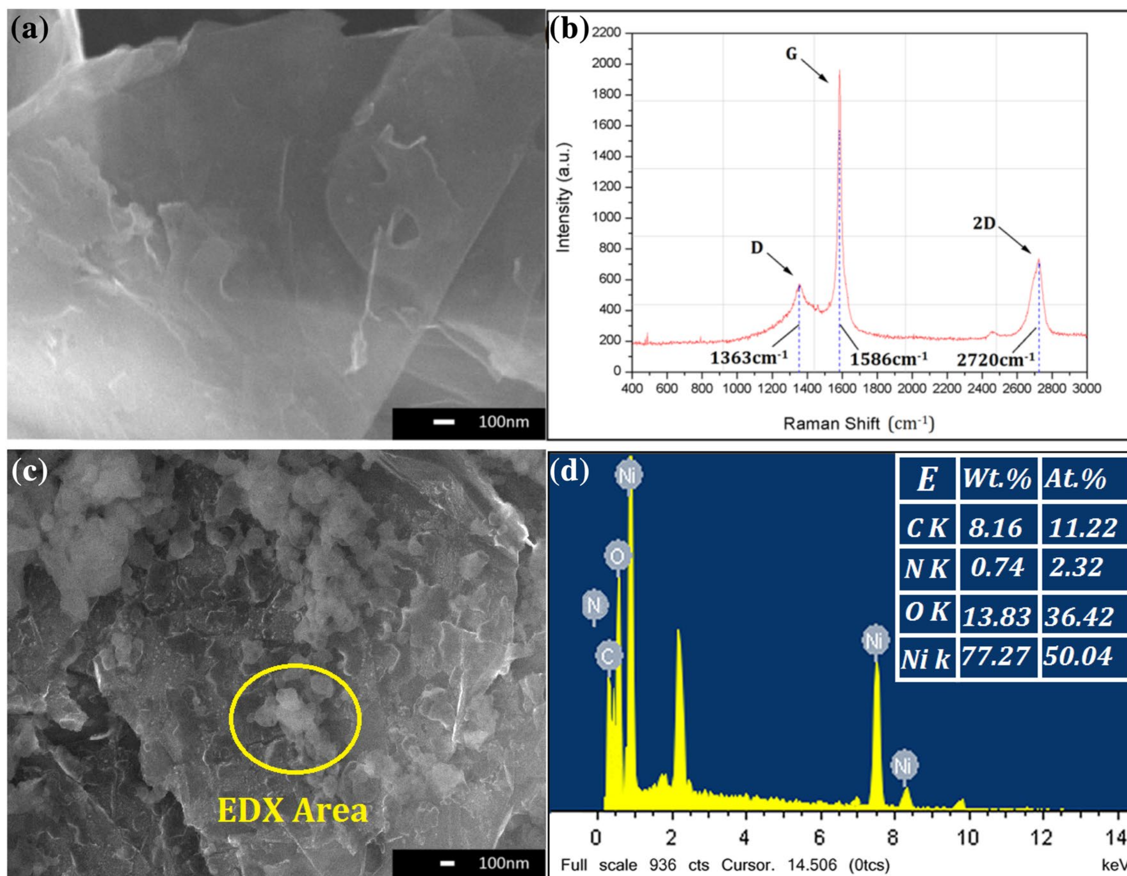

Fig. 1 **a** As-purchased GNS, **b** Raman spectrum of GNS, **c** As-prepared Ni-GNS, **d** EDX pattern of chosen location

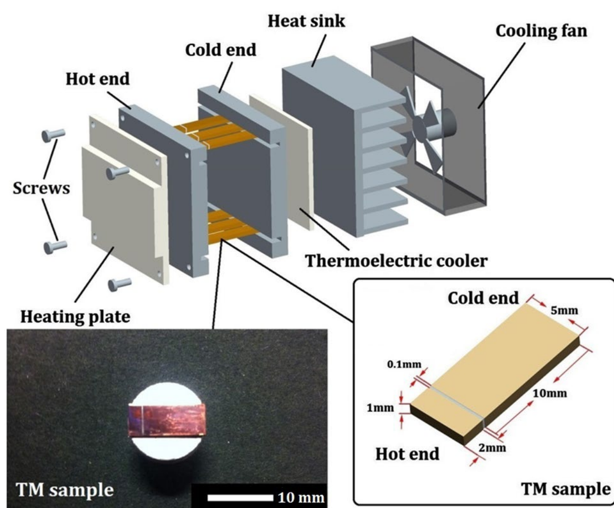

Fig. 2 Schematic diagrams of TM setup and TM sample

as a heat conductor. The spacing between two Cu bases being maintained at 10 mm, while rectangular grooves with a depth of 1 mm were made on inner surfaces of both Cu bases to place TM samples.

The TM sample was designed as an asymmetrical structure with a longer cold end (10 mm) and a shorter hot end (2 mm) owing to the difference of coefficients of heat conduction between the different materials in the Cu/solder/Cu structured sample. The dimensional details of the TM sample are shown in Fig. 2. To prepare a TM sample, the end surfaces of the Cu substrates of both sides were well polished before soldering. A cut solder foil with size of 5 mm × 1 mm × 0.1 mm was then clamped between two Cu substrates using a lab-made clamp. Finally, the clamped Cu substrates and the solder foil, together with the clamp, were placed in a reflow oven to prepare a sandwich-like TM sample with a solder joint width of 100 µm; the reflow profile was presented in Fig. 3. In the TM tests, the two ends of the TM sample were embedded in the pre-manufactured grooves on both the hot and cold Cu bases. In addition, thermal silicone grease was applied on each surface of contact between each component to ensure good thermal conduction. In order to evaluate the feasibility of the prepared TM system and sample, a high-precision infrared microscope (QFI, MWIR-SE) incorporating a self-calibration system was employed to directly observe the temperature distribution in the solder joint of the TM sample.

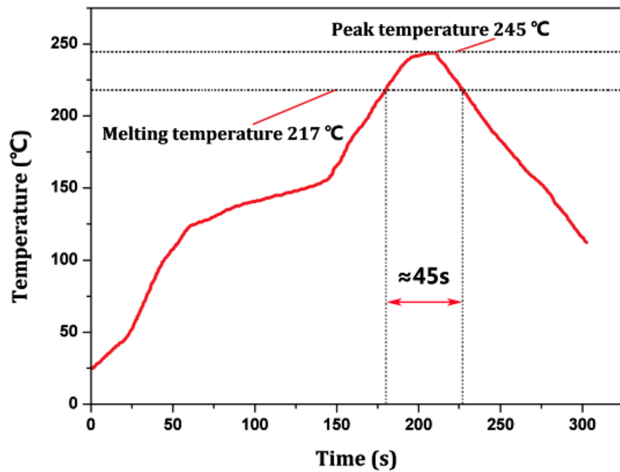

Fig. 3 Reflow profile for preparing TM samples

2.4 Microstructural and compositional characterization

In the TM tests, five samples of each kind of solder were tested for different purposes. Specifically, microstructural evolution of a selected sample for each kind of solder was continuously observed by using a scanning electron microscope (SEM QURTA 200) every 200 h; the total stressing time of the TM tests was designed to take 600 h. The rest of the samples to undergo the same TM stressing process were used for elemental composition analysis. In addition, to quantitatively measure the degree of dissolution of Cu atoms in the solder joints under the current temperature gradient, different solder joints were cut off from the corresponding TM samples after various TM stressing times. After that, the cut solder joints were polished well before being ultrasonically dissolved in aqua regia solution for the purpose of elemental analysis using an inductively-coupled plasma optical emission spectroscope (ICP-OES, Varian-720) with test precision at PPM level.

3 Results and discussion

3.1 Feasibility evaluation of TM setup and sample

The observed temperature distributions for the TM setup and solder joint are shown in Fig. 4a and c. It can be seen from Fig. 4a that there is an obvious temperature difference between the hot and cold ends; the highest and lowest temperatures for the hot and cold Cu bases reached 205.8 and 52.3 °C, respectively. Figure 3c shows the pseudo-color image of part of the solder joint obtained; the actual temperature distribution in the solder joint indicates that the high and low temperature regions of solder joint are mainly located at the hot and cold interfaces, respectively. The highest and lowest temperatures in the solder joint reached 187.5 and 174.6 °C respectively; the average temperature of the whole solder joint was approximately 181.1 °C. To further understand the temperature gradient in the solder joint, three scanning lines (namely, v_1, v_2 and v_3) were randomly selected to measure the temperature distribution across the solder joint; the relevant results are shown in Fig. 5. According to the line-scanned results, it is evident that the collected temperature points in the solder joint exhibit a gradually decreased trend from the hot end through to the cold end. Specifically, the maximum temperatures of v_1, v_2 and v_3 are 186.4, 187.3 and 186.3 °C, while the minimum temperatures of the three tested lines are 174.2, 174.5 and 174.1 °C. Taking into account that the width of solder joint is approximately 100 µm, the temperature differences of these three tested lines are thus calculated as 1220, 1280 and 1220 K/cm, respectively. Accordingly, the average temperature difference across the solder joint is evaluated as 1240 K/cm.

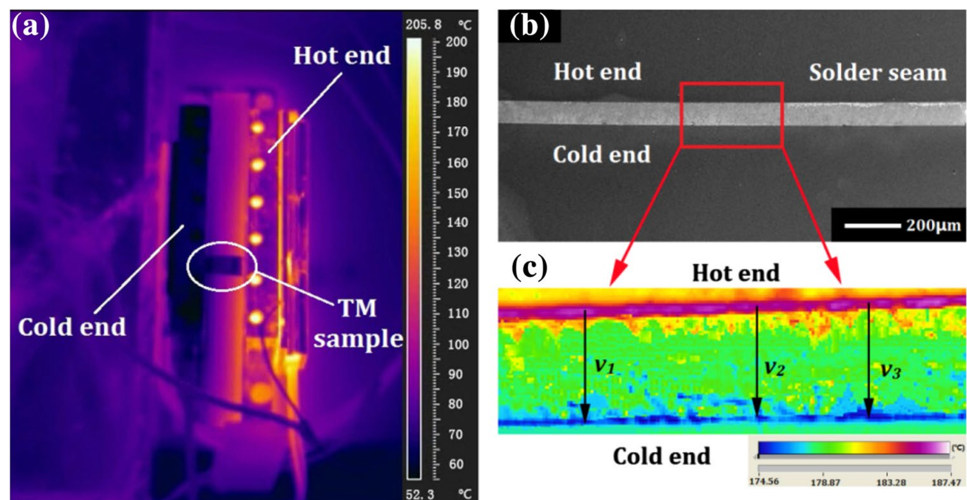

Fig. 4 Temperature distributions in TM setup (**a**) and solder joint (**b**) and (**c**)

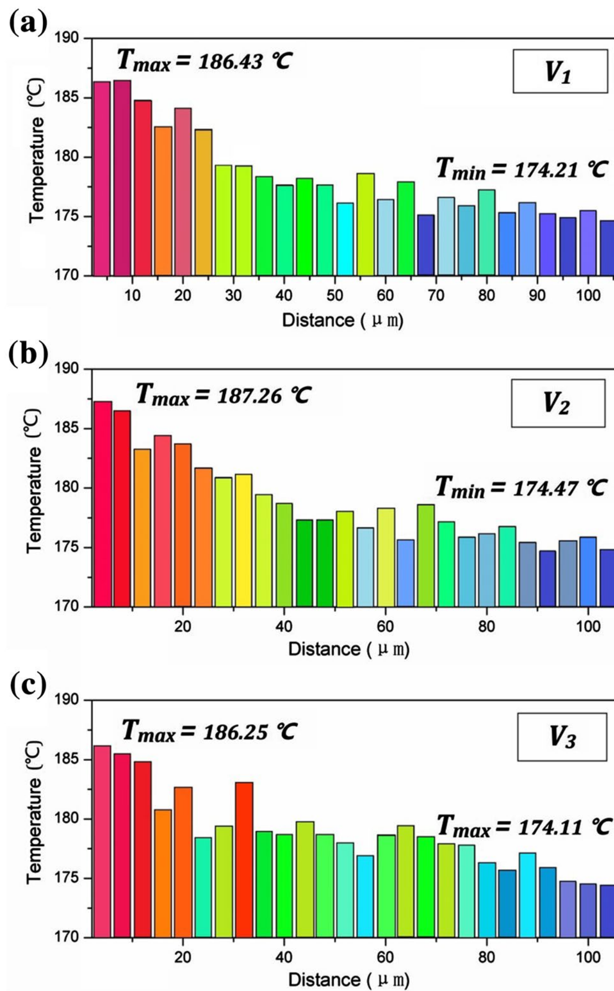

Fig. 5 Actual temperature distribution of V_1, V_2 and V_3 shown in Fig. 4 c

According to previous studies [15], TM in Sn-based solder alloys can be triggered if the environmental temperature and the temperature gradient reach at least 100 °C and 1000 K/cm, respectively. Based on the above-mentioned results, it is apparent that the obtained levels of environmental temperature and temperature gradient in the solder joint effectively meet the requirements for TM. Therefore, the TM setup and the produced sample are viable for use in the TM tests.

3.2 Microstructural evolution

To fully comprehend the effect of TM stressing on the microstructural evolution of both plain and composite solder joints, several kinds of solder joint were observed using SEM before and after TM stressing. The microstructures of two kinds of solder joints before and after different 600 h TM stressing times are shown in Figs. 6 and 8; The results shown in Fig. 6d, e together with Fig. 8d, e were obtained during the stressed condition without the process of polishing and etching being employed.

It can be seen from Fig. 6 that the interfacial IMC at the cold end of the plain SAC solder joint after 600 h of stressing exhibits an obvious increase in thickness, while the IMC at the hot interface had become seriously damaged. In the case of the whole solder joint, the initial smooth surface joint of unstressed SAC had acquired a relatively rough surface with newly-formed patchy IMCs in the central area of the solder joint. In addition, it is worth noting that a thin ridged layer had formed on the interface between the Cu substrate and the Cu–Sn IMC layer (see Fig. 6f); the locally magnified image is shown in Fig. 7a. In order to further verify the composition of both the Cu–Sn IMC and the ridged layer, the interfacial area and six selected points (shown in Fig. 7a) were tested using EDX, the relevant results for which are shown in Fig. 7b and Table 1. According to the EDS mapping result, the ridged layer was derived owing to the presence of Cu, Sn and O. Moreover, the data of elemental compositions of selected points further reveal that the upper layer IMC was Cu_6Sn_5, while the lower ridged lay was Cu_3Sn IMC. The extrusion of Cu_3Sn IMC at the cold interface can be explained by the different migration rate of different atoms. According to the previous report [4], Sn atoms would tend to move to the hot end, while Cu and Ag atoms are more likely to be located at the cold end. Based on this observation, it could be concluded that the stress caused by migration of Cu and Ag atoms (from the hot to the cold end) might be larger than the stress caused by the migration of Sn atoms (from the cold to the hot end), leading to a subsequent pressure stress on the cold interface at the same time as a pressure stress occurs on the hot interface. This stress difference could thus accelerate the damage at the hot end and generate the extrusion of Cu_3Sn IMC at the cold interface. In respect to the composite solder joint reinforced with Ni-GNS, although the thickness of interfacial IMCs at both ends similarly exhibit an increased trend after 600 h TM stressing, no obvious damage at the hot end and no ridged layer was evident at the cold end (see Fig. 8). This phenomenon can be explained thus: when applied, the Ni-GNS reinforcement effectively lowers the diffusion and migration rate of Cu, Sn and Ag atoms, which consequently helps to maintain a relatively stable interfacial microstructure during TM stressing.

To further evaluate microstructural evolution during TM stressing, two kinds of samples after different TM stressing times were polished and etched to facilitate the study of distribution of IMCs in solder joints in conjunction with morphology of interfacial microstructure; the obtained images of which are presented in Figs. 9 and 10. Within the microstructure of the unstressed plain SAC sample, β-Sn, needle-like Ag_3Sn IMC and blocky Cu_6Sn_5 IMC were found to be present in the solder joint. By contrast, in addition to the

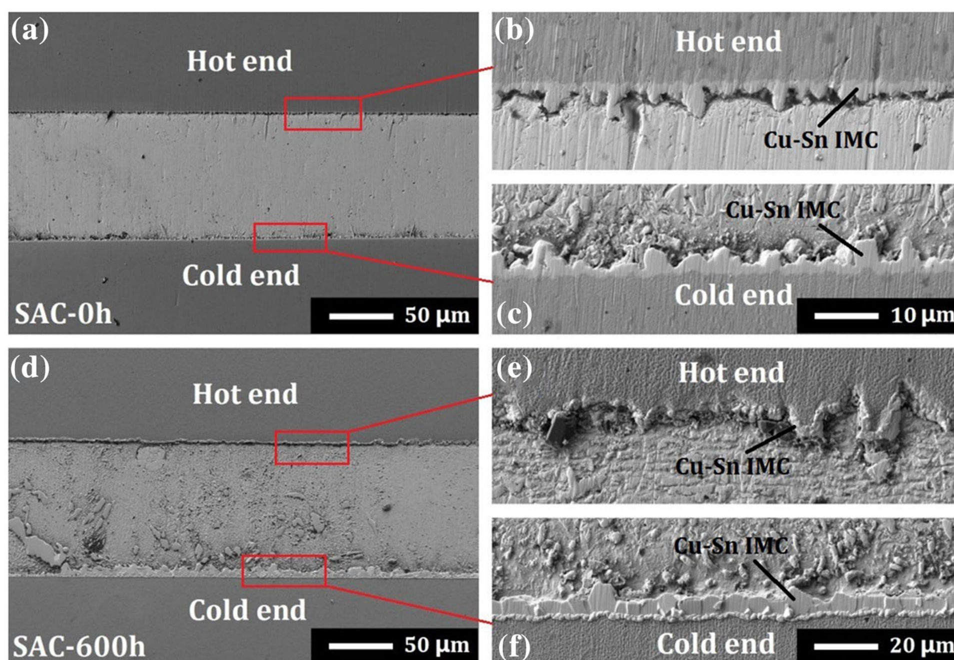

Fig. 6 SAC305 solder joint before (**a**–**c**) and after (**d**–**f**) 600 h TM stressing without polishing and etching

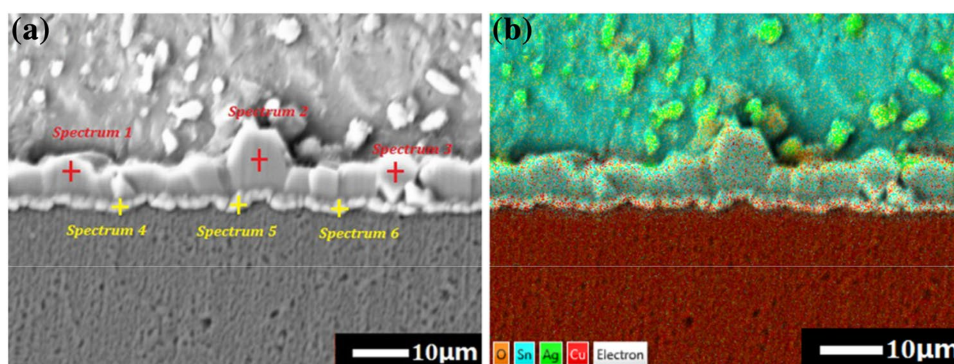

Fig. 7 **a** SEM image of selected cold interface of plain SAC solder joint after 600 h TM stressing and **b** corresponding EDS mapping result

Table 1 Elemental composition (At %) of selected points in Fig. 6a

	Sn	Ag	Cu	O
Spectrum1	41.3	0.3	47.6	10.8
Spectrum2	41.7	0.2	47.9	10.2
Spectrum3	40.8	0.4	46.5	12.3
Spectrum4	21.7	0.2	56.9	21.2
Spectrum5	22.4	0.1	58.7	18.8
Spectrum6	24.3	0.3	63.6	11.8

β-Sn and Ag_3Sn phases, the newly formed Cu–Ni–Sn IMC clusters were also observed in the unstressed composite solder joint. It is also notable that, compared to the initial SAC solder joint, both the size of β-Sn phase and the morphology of Ag_3Sn IMC show a difference in the composite solder joint. Specifically, the average size of β-Sn grain was found to be considerably smaller than in the plain SAC305 solder joint, while the shape of Ag_3Sn IMC had altered in form from a needle-like to granular appearance. The variation of β-Sn in grain size can be explained by the additional Ni-GNS reinforcement providing more nucleation sites during the solidification process; this could also impede the growth of grains by hindering atomic diffusion [21]. Moreover, the variation in shape of Ag_3Sn IMC could be attributed to a change in degree of supercoiling, caused by the incorporation of foreign reinforcement [16].

With an increase in TM stressing time, large quantities of bulky Cu–Sn IMCs can be found in plain SAC solder joints (see Fig. 9); these Cu–Sn IMCs consist of the original Cu_6Sn_5 present in the SAC305 solder and the newly formed Cu_6Sn_5 as a result of dissolution and migration of Cu atoms emerging from Cu substrates. Compared to the plain SAC solder joint, the microstructure of the Ni-GNS reinforced composite solder joint also takes on a different appearance under various TM stressing times; the original Cu–Ni–Sn

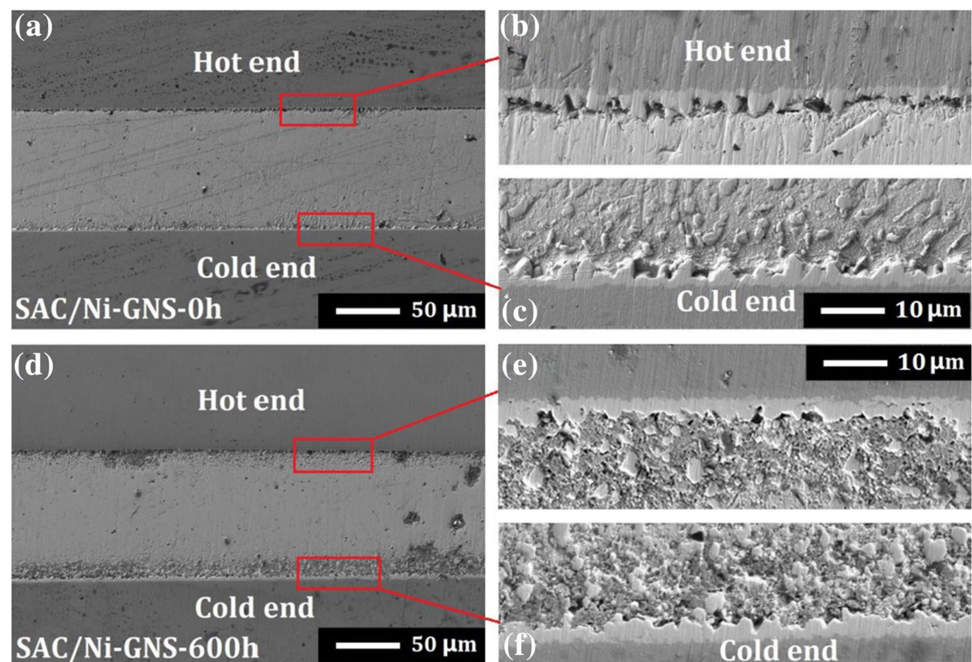

Fig. 8 SAC305/0.1Ni-GNS composite solder joint before (**a**–**c**) and after (**d**–**f**) 600 h TM stressing without polishing and etching

IMCs in the composite solder joint become much larger and more plentiful after TM stressing (see Figs. 10a, d, g and j). This growth might also be attributed to the reaction between the Ni nanoparticles deposited on the GNS surface and the solder matrix due to ageing. Moreover, the Cu atoms in the original solder itself together with the Cu atoms dissolved from Cu substrates may also take on a contributory role. In the case of the plain SAC305 solder joint, it was observed that Cu–Sn IMCs appeared primarily at the hot end and the central position of the solder joint after 200 h stressing. As the stressing time continued, the amount of Cu–Sn IMCs continued to increase, and these IMCs were also gradually distributed throughout the entire solder joint (after 400 h stressing). After 600 h TM stressing, the majority of Cu–Sn IMCs were found to be located at the cold end and the central position of the solder joint. In contrast, after 200 h TM stressing, some newly formed Cu–Ni–Sn IMCs clusters were found to be present in the composite solder joint; although most of these IMCs were also formed close to the hot end of the composite solder joint. Their size and morphology were much different to the newly formed Cu–Sn IMCs in the plain SAC solder joint. The newly formed Cu–Ni–Sn IMCs had the appearance of irregular shaped clusters. Furthermore, these IMCs were more inclined to grow on the original basis (see Figs. 10a, d). There was also a marked difference in microstructures between solder joints after 400 and 600 h of TM stressing respectively. In contrast to the obvious evolution process (that of formation, growth and migration) of Cu–Sn IMCs in the plain SAC solder joint, the size and quantity of Cu–Ni–Sn IMCs increase continuously, and their locations in the composite solder joint were not particularly evident over time. It is necessary to point out that the size and distribution of the newly formed Cu–Ni–Sn IMCs in the composite solder joint were not uniform; this phenomenon might be caused by an uneven distribution of Ni-GNS added in the composite solder joint following a process of reflow.

In addition to the different microstructural evolution between the two solder joints, the two types of samples also display difference in growth characteristics of interfacial IMCs during TM stressing. In respect to the plain solder joint, the thickness of interfacial IMCs at the cold end evidently increased in line with the stressing time. The measured data for thickness plotted in Fig. 11a also confirmed this trend; the thickness of interfacial IMCs at the cold end increased almost by three times after 600 h of stressing, growing in size from the initial 2.12–8.96 μm. Correspondingly, the evolution of interfacial IMCs at the hot end is also noteworthy. It can also be seen from Fig. 9 that the thickness of interfacial IMCs at the hot end similarly showed a gradually increase in trend during the first 400 h of stressing; the thickness increasing from 2.51 to 3.36 μm, as shown in Fig. 11a. However, the thickness variation of interfacial IMCs at the hot end was not that pronounced when compared to the cold end. It was also observed that some Kirkendall voids were present in interfacial IMCs at the hot end after 400 h of TM stressing (see Fig. 9i). After 600 h of stressing, it was evident that the original interface had become severely damaged at the hot end; only a very thin layer of IMC remained on the Cu substrate. The interfacial damage at the hot end can be attributed to considerable diffusion and migration of Cu atoms from the substrate into the solder joint during

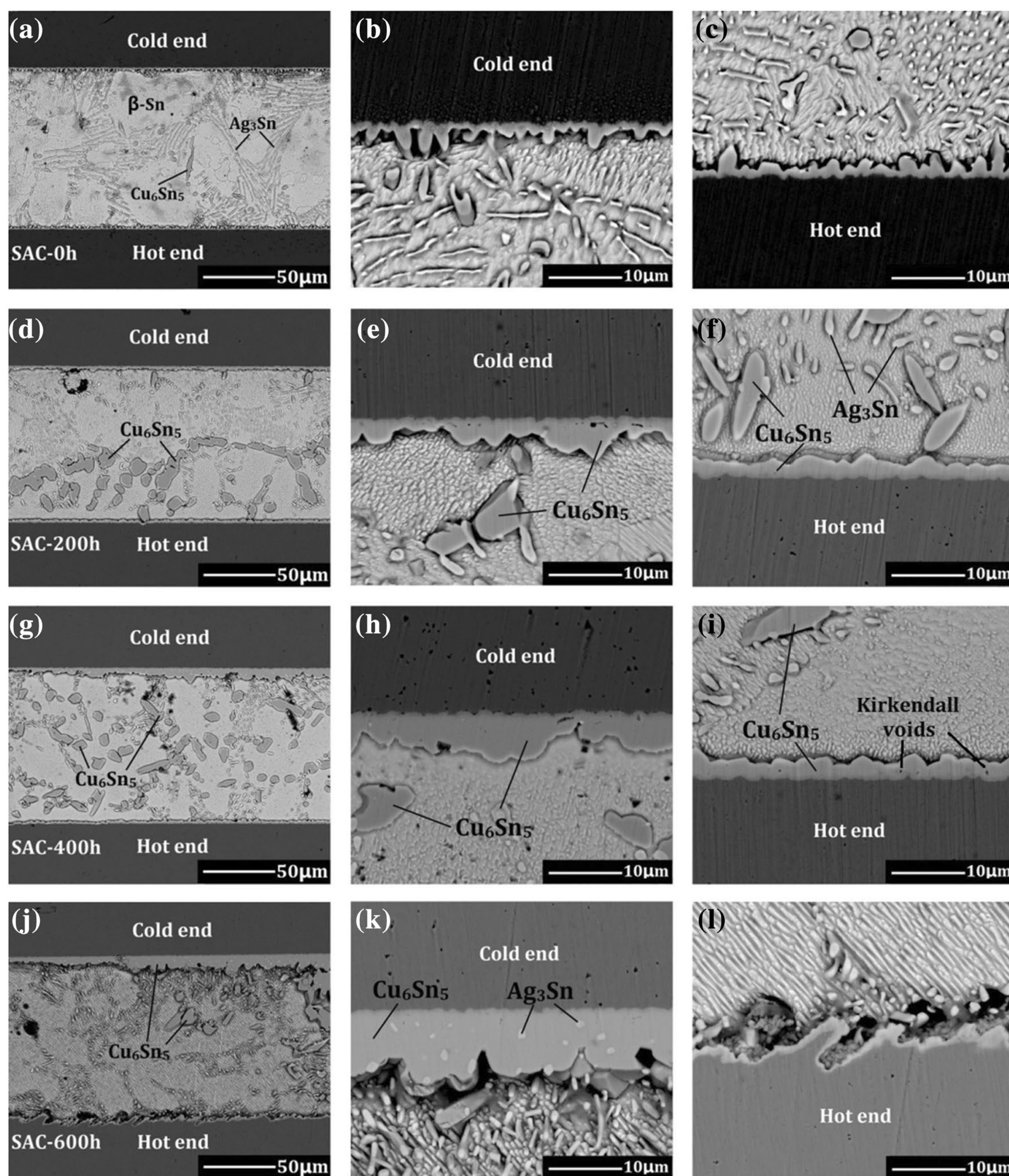

Fig. 9 Microstructural evolution of SAC305 solder joint under temperature gradient of 1240 K/cm: **a–c** initial; **d–f** 200 h; **g–h** 400 h; **j–l** 600 h

the TM stressing process; this interfacial damage had also in turn blocked the pathways for further diffusion of Cu atoms. In addition, some granular Ag_3Sn phase with a light gray color was found in the Cu_6Sn_5 interfacial IMC at the cold end after 600 h of TM stressing. The observed formation, migration and location of Cu–Sn and Sn–Ag IMCs in the SAC305 solder joint during TM stressing indicate that both Cu and Ag atoms migrate from the hot end to the cold one owing to the large temperature gradient; the findings in this study are therefore fully consistent with the current research results obtained by other researchers [4, 22].

In comparison to the plain solder joint, the growth of interfacial IMCs in the composite solder joint was suppressed significantly during TM stressing. Specifically, the thickness of interfacial IMCs at the cold end similarly increased in line with the stressing time, from an initial 2.23–5.16 μm after 600 h (Fig. 11b); this increment in thickness was only 131%, which is considerably less than

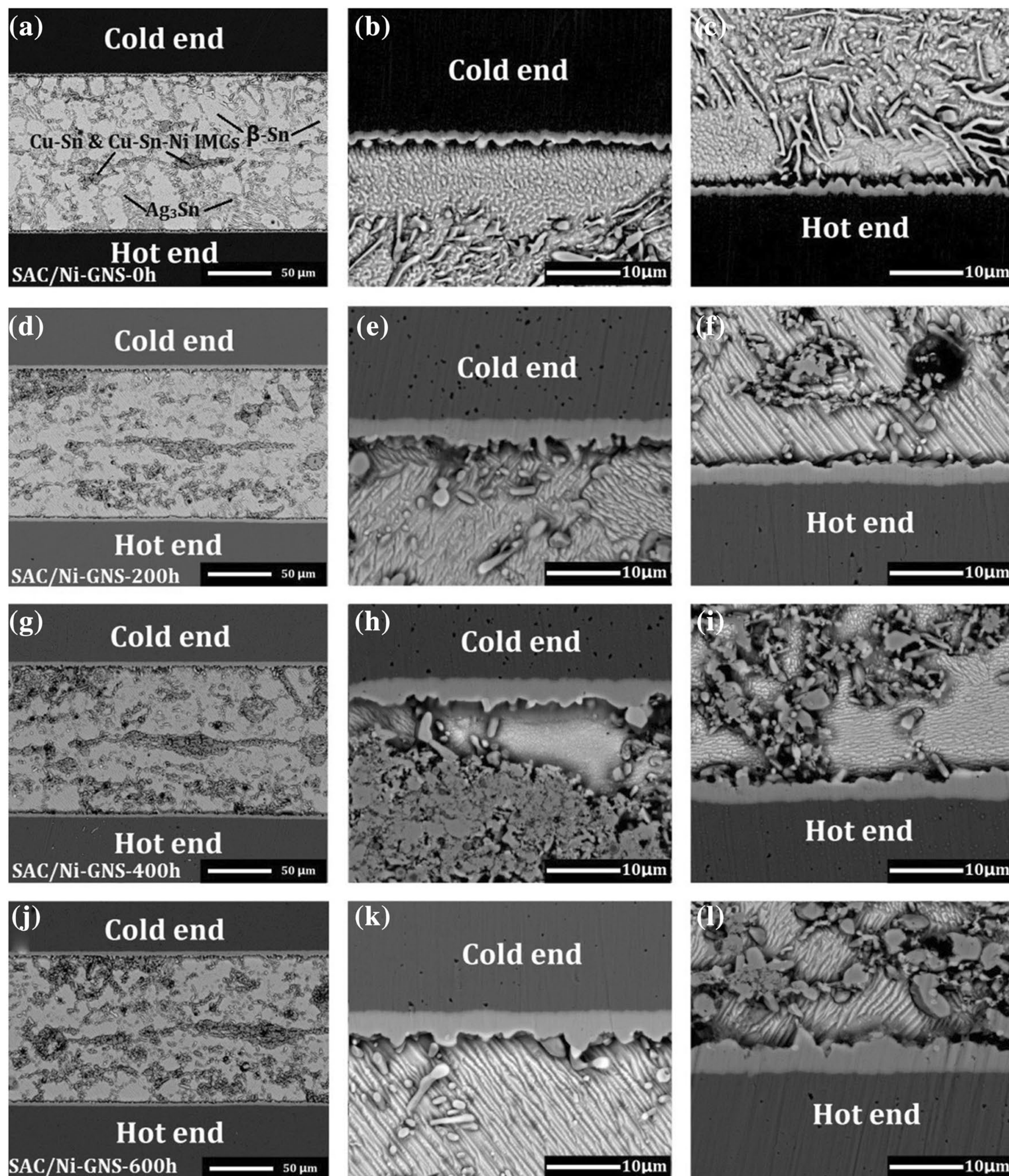

Fig. 10 Microstructural evolution of SAC305/0.1Ni-GNS composite solder joint under temperature gradient of 1240 K/cm: **a**–**c** original; **d**–**f** 200 h; **g**–**i** 400 h; **j**–**l** 600 h

that found in the plain solder joint under the same conditions. Moreover, no Ag_3Sn phase was found in interfacial IMCs at the cold end after 400 or 600 h of TM stressing. As regards the hot end, the thickness of interfacial IMCs similarly increased in accordance with stressing time, from an initial 2.48–5.78 μm after 600 h. However, in contrast to the severe damage occurring at the hot interface of the unreinforced solder joint, interfacial IMCs at the hot end of the composite solder joint remained undamaged, even after 600 h stressing. This therefore suggests that the dissolution process of the Cu substrate, formation and migration of Cu–Sn IMCs together with the growth of interfacial IMCs were all effectively inhibited by the addition of the Ni-GNS reinforcement. According to the microstructural comparison between the plain and composite solder joints after TM stressing, the mitigation of growth and migration of IMCs in the composite solder joint can be explained as follows: The Ni-GNS is a composite reinforcement with a core–shell

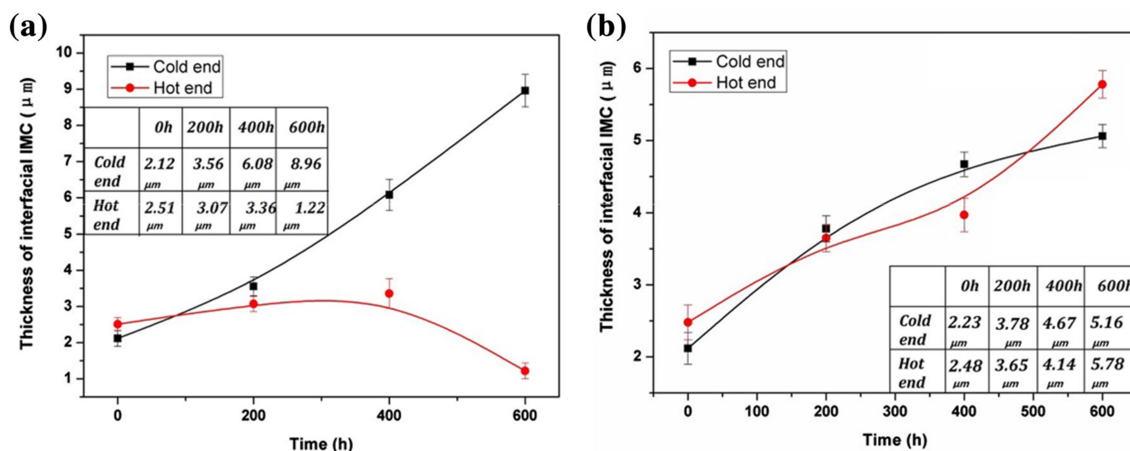

Fig. 11 Evolution of thickness of Cu–Sn IMCs at the Cu/SAC305/Cu (**a**) and Cu/SAC305–Ni-GNS/Cu (**b**) with TM stressing time

structure, more specifically, the inner GNS nanosheets and the outer decorated Ni nanoparticles. During TM stressing, the partially reacted Ni in the composite solder joint would continue to react with the Sn atoms, with the Cu atoms coming from the Cu substrate, leading to a progressive formation and growth of Cu–Ni–Sn IMCs. This process could consume most of the Cu atoms that dissolved from the Cu substrate at the hot end; the dissolved Cu atoms were retained in the composite solder joint in the form of Cu/Ni-containing IMCs, thereby mitigating the further diffusion and migration of Cu atoms from the hot end to the cold end. A further observation is that the inner GNS nanosheets can serve as an additional barrier, to also hinder the diffusion of Cu atoms as well as the migration of IMCs, leading to a more stable interface in the composite solder joint during TM stressing.

To evaluate the influence of doping of Ni-GNS on diffusion of Cu atoms from the Cu substrate to the solder joints, the weight fractions of Cu in the solder joints were quantitatively tested for different TM stressing periods using ICP-OES. In the ICP tests, four treated samples were selected for all types of solder in order to improve the testing accuracy. The average Cu content for each solder was used as the testing result for comparative analysis; the ICP results are shown in Fig. 12. Despite the likelihood of some errors owing to the cutting and polishing processes in measuring the content of Cu in the solder joints, the results obtained still revealed a clear difference in the Cu content in two types of solder joints after different periods of stressing had elapsed. Specifically, the weight percentages of Cu had increased in both solder joints as the TM stressing time increased; however, the increase rate in the plain SAC305 solder joint was much higher than that in the composite solder joint throughout the entire stressing process. After 600 h of stressing, the average Cu content in the former sample reached 4.55 wt%, about nine times higher than its initial value of 0.52 wt%. In contrast, the average Cu content in

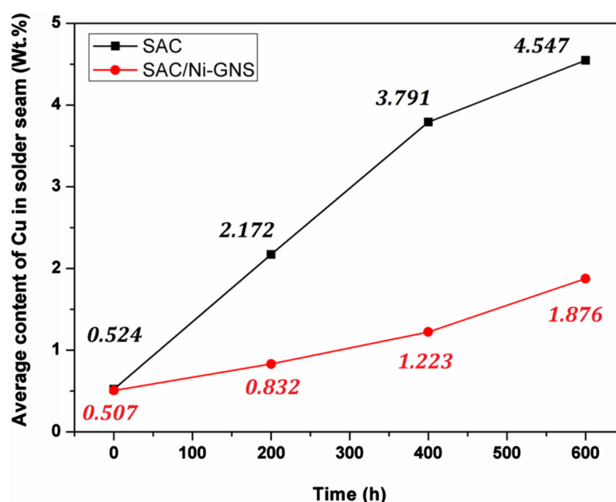

Fig. 12 Evolution of weight percentage of Cu in solder joints with stressing time

the composite solder joint after 600 h stressing was 1.88 wt%; approximately only four times higher than its initial value of 0.51 wt%. It is worth noting that the increase rate of Cu in the plain SAC305 showed a decreasing trend in the interval between 400 and 600 h. This phenomenon can be explained by the fact that the diffusion and migration paths of Cu atoms at the Cu/solder interface were damaged owing to a long-term TM stressing (see Fig. 9l). To avoid the issue caused by the above-described phenomenon, only the data for times below 400 h were used to calculate the dissolution rate of Cu atoms during the testing of TM stressing. Thus, the dissolution rate of Cu can be calculated employing the formula as follows:

$$v = \frac{M(w_2 - w_1)}{T} \tag{1}$$

where v is the dissolution rate of Cu atoms, M is the average weight of the solder joint, T is the stressing time, w_1 and w_2 are the weight fractions of Cu in the solder joints after 0 and 400 h of stressing, respectively. After 400 h stressing, the net increase of Cu in the SAC305 solder joint was 3.27 wt%; since the weight of the solder joint was approximately 38, and 1.24 mg of Cu was dissolved into the solder joint during 400 h of stressing. As the experimental parameters, including the temperature gradient and environmental temperature within the solder joint were relatively stable, the dissolution rate of Cu atoms forming on the substrate to the solder joint can thus be calculated as 3.1×10^{-6} g/h. Conversely, the increment of Cu content was only 0.272 mg in the composite solder joint after 400 h stressing; the dissolution rate of Cu atoms was calculated as 0.68×10^{-6} g/h, and was notably lower than that found in the plain solder joint. The ICP results and the calculated dissolution rates of Cu atoms indicate that the addition of Ni-GNS reinforcement helps to mitigate the diffusion from the Cu substrate into the solder joint under TM conditions.

4 Conclusions

Lead-free composite solder (SAC305/0.1Ni-GNS) was prepared using the process of powder-metallurgy. A system was designed and corresponding samples prepared for TM testing; the obtained temperature gradient in the solder joint based on this procedure was 1240 K/cm. After TM stressing, considerable diffusion of Cu from the substrate to the solder joint was found in the plain SAC solder joint, while a continuous growth in size and quantity of Cu–Ni–Sn IMCs was observed in the composite solder joint. After 600 h of stressing, the interface of plain SAC solder joint at the hot end was seriously damaged, while a significant increase in the thickness was found in interfacial IMCs at the cold end. Although interfacial IMCs in the composite solder joint also exhibited an increasing trend during TM stressing, the interfacial microstructure at both ends remained undamaged. According to ICP results, the dissolution rate of Cu in the plain SAC305 solder under the current experimental conditions was 3.1×10^{-6} g/h, as opposed to that for the composite solder which was only 0.68×10^{-6} g/h. The findings of this study reveal that the incorporation of Ni-GNS could effectively mitigate the negative impact of TM; thus indicating that composite solders which contain Ni-GNS reinforcement have a greater potential for application under harsh service conditions.

Acknowledgements This work was supported by the National Nature Science Foundation of China (Grant No. 61574068), the Fundamental Research Funds for the Central Universities (No. 2016JCTD112) and the Marie Curie International Research Staff Exchange Scheme Project within the 7th European Community Framework Programme (Grant No. PIRSES-GA-2010-269113). The author would also like to thank the Analytical and Testing Centre at Huazhong University of Science Technology as well as LMCC at Loughborough University for their analytical and testing services.

Open Access This article is distributed under the terms of the Creative Commons Attribution 4.0 International License (http://creativecommons.org/licenses/by/4.0/), which permits unrestricted use, distribution, and reproduction in any medium, provided you give appropriate credit to the original author(s) and the source, provide a link to the Creative Commons license, and indicate if changes were made.

References

1. E.M.N. Ervina, S. Amares, T.C. Yap, Solder. Surf. Mt. Technol. **25**, 229 (2013)
2. X. Hu, W. Chen, B. Wu, Mater. Sci. Eng. A **556**, 816 (2012)
3. Y. Li, K. Moon, C.P. Wong, Science **308**, 1419 (2005)
4. C. Chen, H.Y. Hsiao, Y.W. Chang, F.Y. Ouyang, K.N. Tu, Mater. Sci. Eng. R **73**, 85 (2012)
5. C. Basaran, M.F. Abdulhamid, Mech. Mater. **41**, 1223 (2009)
6. C. Chen, H.M. Tong, K.N. Tu, Annu. Rev. Mater. Res. **531**, 40 (2010)
7. L.L. Gao, S.B. Xue, L. Zhang, Z. Sheng, F. Ji, W. Dai, S.L. Yu, G. Zeng, Microelectron. Eng. **87**, 2025 (2010)
8. L.C. Tsao, S.Y. Cheng, C.W. Chen, T.Y. Chen, Mater. Sci. Eng. A **159**, 658 (2016)
9. D.L. Ma, P. Wu, J. Alloy Compd. **580**, 127 (2016)
10. M. Sobhy, A.M. El-Refai, M.M. Mousa, G. Saad, Mater. Sci. Eng. A, **646**, 82 (2015)
11. S. Chellvarajoo, M.Z. Abdullah, Z. Samsudin, Mater. Des. **67**, 197 (2015)
12. R. Zhao, L.M. Ma, Y. Zuo, S.H. Liu, F. Guo, J. Electron. Mater. **42**, 280 (2013)
13. X. Hu, Y.C. Chan, K.L. Zhang, K.C. Yung, J. Alloy Compd. **580**, 162 (2013)
14. A.T. Huang, A.M. Gusak, K.N. Tu, Y.S. Lai, Appl. Phys. Lett. **88**, 141911 (2006)
15. F.Y. Ouyang, C.L. Kao, J. Appl. Phys. **110**, 123525 (2011)
16. G. Chen, F.S. Wu, C.Q. Liu, V.V. Silberschmidt, Y.C. Chan, J. Alloy Compd. **656**, 500 (2016)
17. A. Lee, K.N. Subramanlan, J. Electron. Mater. **34**, 1399 (2005)
18. L. Zhang, C.W. He, Y.H. Guo, J.Q. Han, Y.W. Zhang, X.Y. Wang, Microelectron. Reliab. **52**, 559 (2012)
19. J. Shen, Y.C. Chan, Microelectron. Reliab. **49**, 223 (2009)
20. A.C. Ferrari, J. Robertson, *Raman Spectroscopy in Carbon: From Nanotubes to Diamond*. (Royal Society Press, London, 2004)
21. G. Chen, F.S. Wu, C. Liu, W. Xia, H. Liu, Mater. Sci. Eng. A **636**, 484 (2015)
22. H.B. Huntington, in: *Diffusion*, ed. by H.I. Aaronson. *Handbook on the Physics and Chemistry of Rare Earths*, Chap. 6 (American Society for Metals, Metals Park, 1973)